



**University of
Sunderland**

Xiaohui, Fua, Vin Cent, Taib, Lip Kean, Moey, Nor Faiza Abd, Rahmand, Kamarul Arifin, Ahmad and Baglee, David (2024) Opening configurations and natural cross ventilation performance in a double-loaded multi-level apartment building: A CFD analysis. *Building and Environment*, 254. ISSN 0360-1323

Downloaded from: <http://sure.sunderland.ac.uk/id/eprint/17485/>

Usage guidelines

Please refer to the usage guidelines at <http://sure.sunderland.ac.uk/policies.html> or alternatively contact

sure@sunderland.ac.uk.

1 **Opening Configurations and Natural Cross Ventilation**
2 **Performance in a Double-loaded Multi-level Apartment Building: A**
3 **CFD Analysis**

4 *Xiaohui Fu ^{a,b,e}, Vin Cent Tai ^{b,*}, Lip Kean Moey ^b, Nor Faiza*

5 *Abd Rahman ^b, Kamarul Arifin Ahmad ^c, David Baglee ^d*

6 *^a School of Architecture and Civil Engineering, Anhui*

7 *Polytechnic University, Wuhu 241000, China*

8 *^b Centre for Modelling and Simulation, Faculty of Engineering,*

9 *Built Environment & Information Technology, SEGi University,*

10 *47810, Selangor, Malaysia*

11 *^c Department of Aerospace Engineering, Faculty of*

12 *Engineering, Universiti Putra Malaysia, Serdang, Selangor*

13 *43400, Malaysia*

14 *^d School of Engineering, Faculty of Technology, University of*

15 *Sunderland, SRI 3SD Sunderland, United Kingdom*

16 *^e Engineering Research Center of Anhui Green Building and*

17 *Digital Construction, Anhui Polytechnic University, Wuhu*

18 *241000, China*

19

20 ** taivincent@segi.edu.my*

21

22 **ABSTRACT**

23

24 *This study investigates the impact of varied opening configurations on natural*

25 *cross ventilation of a double-loaded multi-level apartment. Using computational*

1 *fluid dynamics (CFD) simulations, twenty-five building models with combinations*
2 *of top-top (TT), top-bottom (TB), center-center (CC), bottom-bottom (BB), and*
3 *bottom-top (BT) opening configurations were analyzed in both windward and*
4 *leeward building blocks. In the windward block, the BB configuration yielded the*
5 *highest dimensionless flow rate (DFR) for levels 1-3, and BT was highest for levels*
6 *5 and 6. Air Exchange Efficiency (AEE) was optimal at 45-55% for TB*
7 *configurations on levels 1-3, and for CC and BT on levels 4-6. Factor optimization*
8 *(α) was introduced to balance DFR and AEE, favoring TB configurations for level*
9 *1-3 and BT configurations for levels 4-6. Additionally, the leeward block's*
10 *ventilation was slightly influenced ($\pm 3.5\%$) by the windward block's*
11 *configurations. Notably, the TT configuration achieved the highest α score at level*
12 *1 and TB at level 2, even with the lowest DFR. Conversely, the CC configuration,*
13 *while having the lowest AEE for the first two levels, yielded the highest DFR*
14 *values. Bottom inlet configurations recorded the lowest α scores for levels 3-6.*
15 *The research suggests that the TT and CC configurations are the most effective for*
16 *ventilation in the leeward block. The results indicate that building design can be*
17 *optimized for ventilation performance at each level without significant impact to*
18 *adjacent structures. This informs improved ventilation strategies in high-rise*
19 *buildings, emphasizing design adaptability to enhance indoor air quality.*

20

21 **Keywords:** *Natural cross ventilation, opening configuration, multi-level building,*
22 *air exchange efficiency, sustainable building*

23

24

25

1

2

3

4

5 **Nomenclature**

A_o	Opening area [m ²]
C_p	Pressure coefficient [-]
F_S	Factor of Safety
H	Height of building [m]
h	Height of room [m]
k	Turbulent kinetic energy [m ² /s ²]
k/U_H^2	Dimensionless ratio of turbulent kinetic energy over the square of the reference velocity [-]
L	Length of building [m]
p	Formal order of accuracy [-]
r	Linear grid refinement factor [-]
U	Streamwise velocity [m/s]
U_H	Reference velocity [m/s]
V_M	Mean streamwise velocity [m/s]
\dot{V}	Volume flow rate through the building [m ³ /s]
W	Width of building [m]

6

7 *Greek Letter*

α	Factor-optimization [-]
ε	Turbulence dissipation rate [m ² /s ³]

κ	Von Karman constant [-]
$\bar{\tau}_r$	Residence time [s]
$\langle \tau_a \rangle$	Volume average age of air [s]
μ	Dynamic viscosity of air [Pa·s]

1 *Abbreviations*

AEE	Air Exchange Efficiency [%]
AOA	Age of Air [s]
BOI	Body of Influence
CFD	Computational Fluid Dynamics
DFR	Dimensionless Flow Rate
FAC2	Factor of two of observation
GCI	Grid Convergence Index
RANS	Reynolds Averaged Navier-Stokes
RKE	Realizable k- ϵ
RMSE	Root Mean Square Error
UDS	User Defined Scalar

2

3

1 **1. Introduction**

2 The rate of global urbanization has risen from 24% in 1950 to 55% in 2018, and
3 is projected to reach 68% by 2050 (Zou et al., 2022). This urbanization trend has
4 fueled the demand for residential buildings, intensifying the use of energy-
5 intensive equipment like air conditioning, heating, and lighting, thereby
6 heightening the energy consumption and environmental burden. In the United
7 States, the heating, ventilation, and air conditioning (HVAC) systems in residential
8 buildings account for over half of the sector's energy (US Energy Information
9 Administration, 2021). In China, urban residential energy use accounts for 39% of
10 building energy consumption, with space heating and cooling alone accounting for
11 about 15% of the country's total energy consumption (China Association of
12 Building Energy Efficiency(CABEE), 2022; Duan et al., 2023; National Bureau
13 of Statistics, 2022). To combat this, passive environmental technologies such as
14 natural cross ventilation are widely used in apartments to improve indoor air
15 quality and thermal comfort without additional energy expenditure (Kobayashi et
16 al., 2022; Moey, Kong, et al., 2021; Omrani et al., 2017; Spentzou et al., 2019).

17 The design of multi-level apartments has evolved to optimize space in urban
18 settings. However, the contiguous layout of the apartments can impede natural
19 ventilation due to building shading, resulting in poor air circulation and stagnant
20 air pockets in certain areas. Therefore, numerous design strategies have been
21 proposed, such as roofs, wind catchers and courtyards or voids, to improve natural
22 cross ventilation. Studies have shown that these design interventions can
23 significantly improve ventilation performance. Haghighi et al. (2016)
24 demonstrated that combining wind catcher and adsorption chiller could effectively
25 provide natural cooling for multi-level building in both dry and humid climates.

1 Muhsin et al. (2017) highlighted the importance of voids and wind directions on
2 indoor airflows and thermal comfort in multi-level housings with natural cross
3 ventilation in Malaysia. Further research by Kumar and colleagues (2021, 2022)
4 underscored the impact of building features like void, pilotis, and fin sizes on
5 natural ventilation performance. Waheeb & Hemeida, (2022) found that modifying
6 the shape of traditional multi-level residential buildings can lead to better natural
7 ventilation performance, resulting in a significant reduction in energy
8 consumption.

9 In addition to the architectural design strategies, the configuration of openings
10 also plays a crucial role in natural ventilation. Bangalee et al. (2013) found that,
11 given a fixed wall porosity, the flow rate was maximized when the opening was
12 located in the center of the opposite walls, while the room with opening located at
13 the diagonal of the opposite walls experienced a 34% lower ventilation rate.
14 Shetabivash (2015) found that the shape and position of the inlet opening have a
15 major influence on cross ventilation and flow patterns within the building, where
16 horizontal inlet openings with top positioning and the outlet opening with bottom
17 positioning can lead to strong recirculation in rooms. Tominaga & Blocken (2016)
18 found that the diffusion and concentration fields and fluctuations of the pollutants
19 are mainly influenced by the inlet opening position compared to the outlet opening
20 position. Moey and colleagues (2021; 2022) identified that certain opening ratios
21 and positions can significantly improve indoor airflow characteristics and
22 ventilation rates in natural ventilated buildings. Li et al., (2023) revealed that that
23 different opening configurations' ventilation performance for a sheltered three-
24 level high-rise buildings varies across levels. Zhang et al. (2022) and others
25 underscored that the mere increase in the number of openings does not necessarily

1 improve ventilation; rather, the size and positioning, along with the use of louvers,
2 play a pivotal role (Kosutova et al., 2019; Tai et al., 2022; Yazarlou & Barzkar,
3 2022; Zheng et al., 2020).

4 However, the aforementioned studies focus primarily on the impact of opening
5 configurations on natural cross ventilation in a generic one-room single-story
6 building. Zheng et al. (2022), Jiang et al. (2022), and Najafi Ziarani et al.(2023)
7 began addressing the research gap by examining the impact of opening
8 configurations and louvers on natural ventilation in multi-level buildings. All these
9 studies demonstrated the complex interplay of opening configurations on airflow
10 and pollutant dispersion.

11 There are only a few studies that investigated the influence of the opening
12 configuration on natural ventilation on each level for a double-loaded multi-level
13 apartment. Given the inherent complexity of integrating natural ventilation into
14 building design, architects and engineers face the challenges in melding aesthetics
15 with functionality. Building on the work by Kumar et al. (2021), this study
16 modifies the opening sizes and positions to test various configurations using
17 computational fluid dynamics (CFD) simulations. The main objective of this study
18 is to investigate the effect of opening configurations on natural cross ventilation of
19 a double-loaded multi-level apartment. Specifically, indoor ventilation
20 performance such as DFR, AEE, and indoor airflow characteristics are
21 investigated. This research aims to enhance indoor ventilation performance in
22 high-rise urban environments through new insights and knowledge. It is hoped to
23 provide some references for the design of façade openings in double-load multi-
24 level apartments to achieve efficient indoor ventilation performance of the
25 building.

1

2 **2. Methodology**

3 *2.1 Model Geometry and Computational Domain*

4 In this study, the selected building model is based on the studies by (Kumar et
5 al., 2021) and (Shirzadi et al., 2018). The dimensions of the building are scaled
6 down using a ratio of 1:75 relative to the full-scale dimensions. The scaled
7 dimensions of the building model are 600 mm (length) \times 280 mm (width) \times 252
8 mm (height), with a wall thickness of 2 mm. In contrast, the full-scale dimensions
9 are 45 m (length), 21 m (width), and 18.9 m (height). The building comprises two
10 six-story blocks separated by a 3-meter void in the center, as illustrated in Figure
11 1. To simplify the model, only one side unit and one middle unit on each level of
12 both building blocks are considered. Each unit has a window-to-wall ratio of
13 10.16%. The dimension of each opening is 20 mm (width) \times 8 mm (height). As
14 shown in Figure 2, three opening positions are evaluated: bottom, center, and top,
15 measured at 0.25h, 0.5h, and 0.75h from the floor, respectively. Five distinct
16 opening configurations are considered: (i) top-top, (ii) top-bottom, (iii) center-
17 center, (iv) bottom-bottom, and (v) bottom-top. This results in a total of 25
18 numerical cases, based on varying combinations of opening positions, as detailed
19 in Table 1.

20

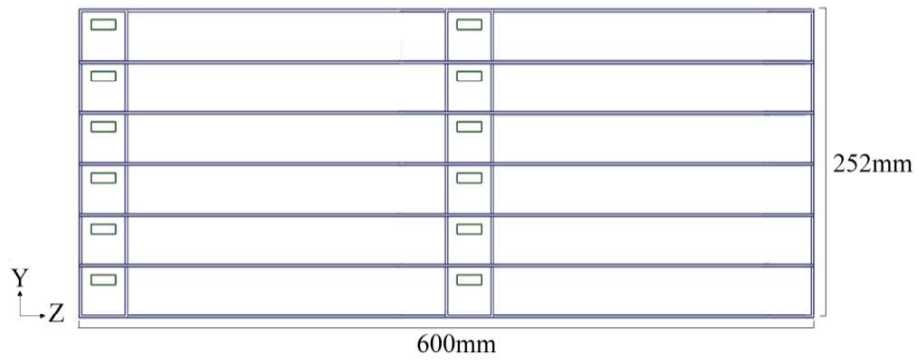
21

Table 1. Simulation cases.

Case	Opening position in block A (inlet-outlet)	Opening position in block B (inlet-outlet)	Case abbreviation
1	Top-Top	Top-Top	A-TT/B-TT
2		Top-Bottom	A-TT/B-TB
3		Center-Center	A-TT/B-CC

4		Bottom-Bottom	A-TT/B-BB
5		Bottom-Top	A-TT/B-BT
6	Top-Bottom	Top-Top	A-TB/B-TT
7		Top-Bottom	A-TB/B-TB
8		Center-Center	A-TB/B-CC
9		Bottom-Bottom	A-TB/B-BB
10		Bottom-Top	A-TB/B-BT
11	Center-Center	Top-Top	A-CC/B-TT
12		Top-Bottom	A-CC/B-TB
13		Center-Center	A-CC/B-CC
14		Bottom-Bottom	A-CC/B-BB
15		Bottom-Top	A-CC/B-BT
16	Bottom-Bottom	Top-Top	A-BB/B-TT
17		Top-Bottom	A-BB/B-TB
18		Center-Center	A-BB/B-CC
19		Bottom-Bottom	A-BB/B-BB
20		Bottom-Top	A-BB/B-BT
21	Bottom-Top	Top-Top	A-BT/B-TT
22		Top-Bottom	A-BT/B-TB
23		Center-Center	A-BT/B-CC
24		Bottom-Bottom	A-BT/B-BB
25		Bottom-Top	A-BT/B-BT

1



(a)

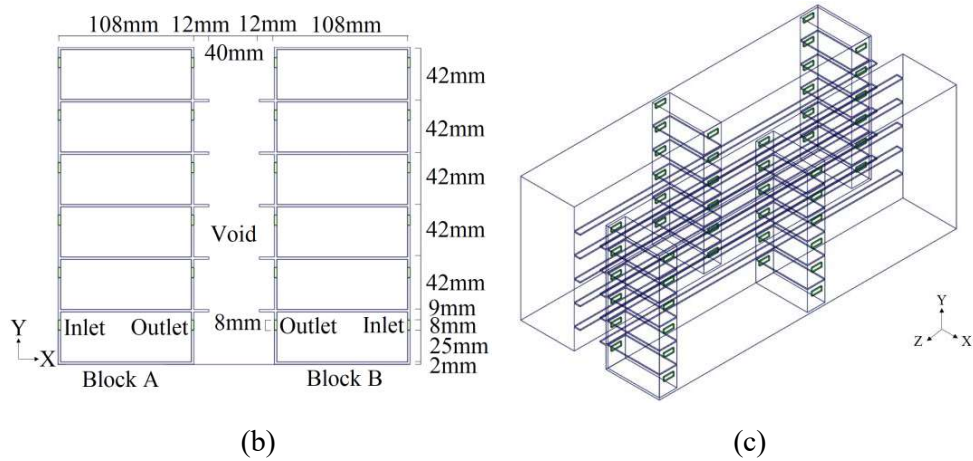


Figure 1. Building geometry. (a) Front, (b) side, and (c) isometric views.

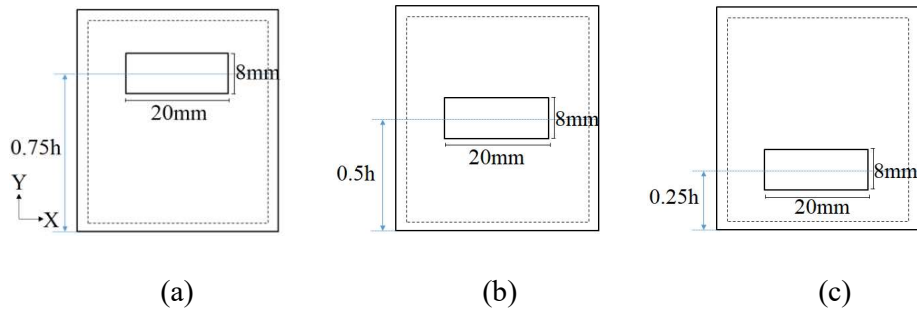


Figure 2. Opening dimensions for (a) top, (b) center, and (c) bottom.

1
2 The computational domain is set up according to (Kumar et al., 2021) (see
3 Figure 3), where the building is located $5H$ from the inlet boundary, $6H$ from the
4 top boundary, and $15H$ from the outlet boundary. This setup follows the guidelines
5 proposed by the Working Group of the Architectural Institute of Japan (AIJ)
6 (Tominaga et al., 2008) and COST (Franke, 2006). However, the lateral boundary
7 is only $2.4H$ from the building, which is less than the recommended $5H$ by AIJ and
8 $2.3W$ (approximately $2.53H$ in this study) by the COST guidelines. Nonetheless,
9 Kumar et al. (2021) confirmed that the lateral distance between the model and the
10 flow domain's sidewalls do not significantly influence the velocity and pressure
11 distributions around the model when compared to the CFD simulation they

1 conducted using an enlarged computational domain with a lateral distance of 5H
 2 (Kumar et al., 2021). The resultant computational domain blockage ratio is less
 3 than 5%. To increase the mesh resolution around the building and the openings,
 4 smaller rectangular domains called body of influences (BOIs) encapsulating the
 5 targeted geometries are added to refine the mesh within the BOIs.
 6

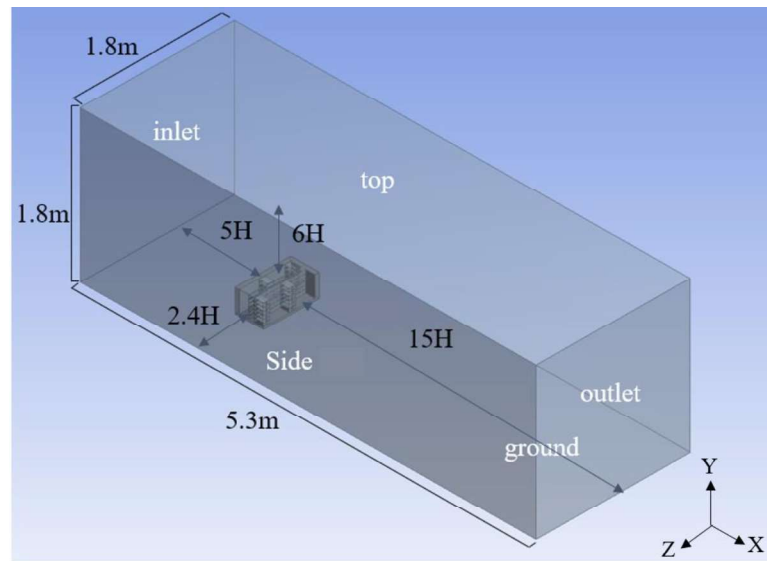


Figure 3. Computational domain.

7

8 2.2 Boundary conditions

9 The inlet boundary conditions for inlet velocity U and turbulent kinetic energy
 10 k profiles in this study are set according to the work by (Kumar et al., 2021), as
 11 depicted in Figure 4. The profile of U follows a power law with an exponent of α
 12 $= 0.25$ described by equation (1), while k is determined based on the measured data
 13 from wind tunnel experiment. The distribution of the turbulent dissipation rate (ϵ)
 14 is calculated according to equation (2) (Tominaga et al., 2008):

$$15 \quad U(y)/U_H = (y/H)^\alpha \quad (1)$$

1
$$\varepsilon(y) = C_{\mu}^{\frac{1}{2}} \kappa(y) \frac{U_H}{H} \alpha \left(\frac{y}{H} \right)^{\alpha-1} \quad (2)$$

2 Where, $C_{\mu} = 0.09$ is the model constant, k is turbulent kinetic energy (TKE). $U_H =$
3 3.95 m/s at the reference height (i.e., the building height) of 0.252 m, and $U(y)$ is
4 the time-averaged streamwise velocity at a height y . The symmetric boundary
5 condition is applied to the top and both sides of the domain, while no-slip condition
6 is applied to the ground.

7 A CFD simulation with the empty domain using the same mesh settings is
8 conducted to test the horizontal homogeneity of the atmospheric boundary layer
9 along the computational domain. The U and k profiles at the incident line situated
10 at 5H downstream from the inlet are compared with the inlet profiles. The results
11 are presented in Figure 4, alongside with experimental results reported in (Kumar
12 et al., 2021). In general, the incident velocity profile agrees well with the inlet
13 profile, indicating no streamwise inhomogeneity for velocity profile. However, the
14 inlet and incident k profiles show streamwise inhomogeneity, where streamwise
15 gradients are formed near the ground at around $y/H = 0.5$. This is consistent with
16 the experimental results by Kumar et al. (2021), where the incident k profile shows
17 a weaker streamwise gradient. Nonetheless, the inhomogeneity is considered
18 acceptable as the k value at $y/H = 1$ is equal to the inlet value (Ramponi &
19 Blocken, 2012).

20

21

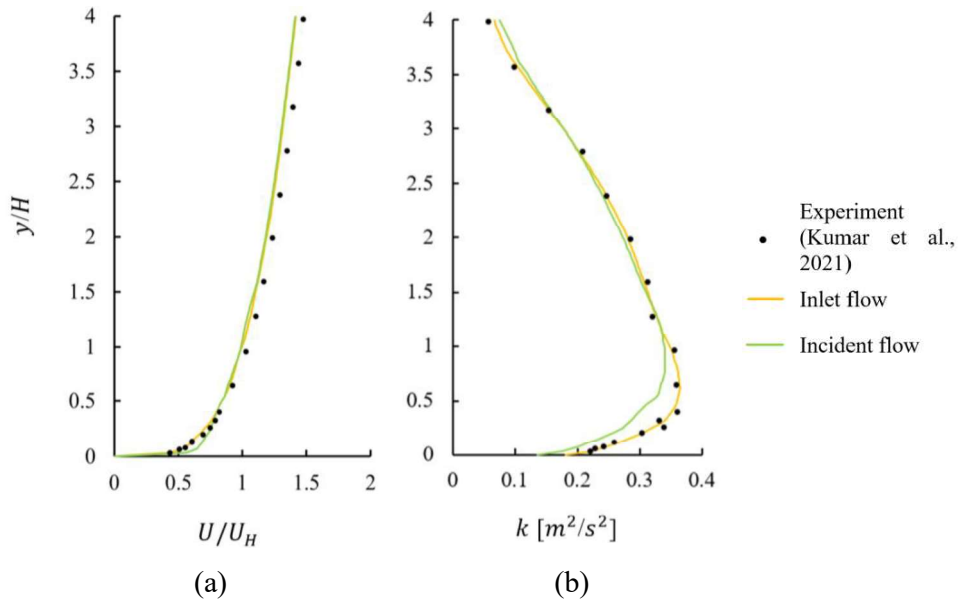


Figure 4. Vertical profiles of (a) U/U_H , and (b) k , measured at domain inlet and incident flow location for the empty-domain case using medium grid.

1

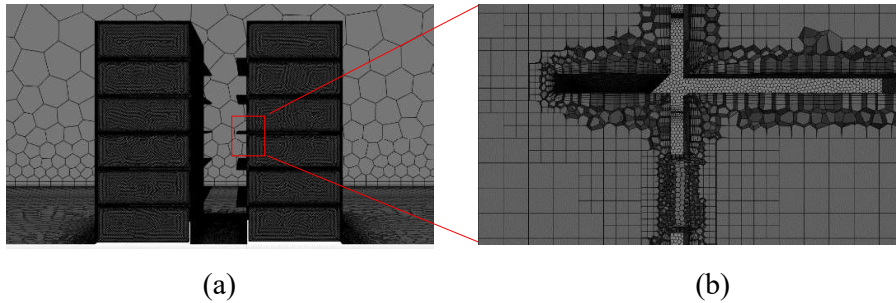


Figure 5. Poly-hexcore mesh. (a) Surface mesh, and (b) prism layers around the building wall.

2

3 The meshing and CFD simulations are conducted using ANSYS 2023 R1. The
 4 dynamic viscosity of air, μ is set to 1.79×10^{-5} Pa \cdot s. Poly-hexcore cells are used
 5 in the meshing, for its ability to give meshes with lower cell count, higher mesh
 6 quality, and better solver efficiency compared to traditional meshing technologies
 7 (ANSYS, 2020). The resultant mesh is presented in Figure 5. Five layers of prism
 8 cells with an expansion ratio of 1.2 are applied to the building walls and ground.
 9 The first cell height is $50 \mu\text{m}$, corresponds to $y^+ \approx 2.5$. The maximum $y^+ \approx 4.5$

1 occurred only on the ground at the corner of the building. The mesh skewness for
2 all numerical cases is controlled not to exceed 0.60.

3

4 2.3 *CFD solver settings*

5 The finite volume approach is employed to solve the governing equations for
6 mass and momentum. The Realizable k - ε (RKE) model from the 3D steady
7 Reynolds Averaged Navier-Stokes (RANS) is employed. The transport equations
8 for all variables are discretized using the second-order upwind scheme for the
9 advection terms, including mass, momentum, k , ε , User Defined Scalar (UDS),
10 and the pressure interpolation is kept at second order. The semi-implicit method
11 for pressure linked equations (SIMPLE) algorithm is used for pressure velocity
12 coupling of the RANS model simulations. Convergence of the simulations is
13 determined based on the scaled residuals of the equations. Specification of
14 convergence criteria depends on the problem under investigation and the desired
15 accuracy of outputs. COST guidelines recommend reducing the scaled residual by
16 4 orders of magnitude (Asfour, 2010; Franke, 2006). In this study, the simulations
17 are considered converged when the scaled residuals leveled off and reached a
18 minimum value of 1×10^{-6} for x, y, and z momentum, and a minimum value of
19 1×10^{-4} for k , ε , and continuity, and a minimum value of 1×10^{-5} for UDS
20 residuals.

21

22 2.4 *Mesh sensitivity analysis and model validation*

23 In the grid sensitivity analysis conducted using the RKE model with Enhanced
24 Wall Treatment, three different grid sizes are used: coarse, medium, and fine
25 meshes. It is created by refining and coarsening the medium grids by a factor of

1 approximately $\sqrt{2}$ in each direction. For medium mesh, the mesh size for walls and
2 openings was set at 35 mm and 5 mm, respectively. The total number of elements
3 is from 8,342,066 to 12,866,647 and 18,830,076 for the coarse, medium, and fine
4 meshes, respectively.

5 The grid convergence index (GCI) by Roache is employed to estimate the error
6 in the results for each mesh size as shown in Equation (3) (Kosutova et al., 2019;
7 Kumar et al., 2022; Liu et al., 2018; Roache, 1997; Tai et al., 2022; van Hooff et
8 al., 2017). Table 2 shows the average GCI for the three mesh types for Lines A, B,
9 C, D, and E. As shown in Figure 6, lines A and E are located at the center of rooms,
10 and lines B and D are located at the inside of the internal walls. Meanwhile, line C
11 is in the middle of vertical void.

$$12 \quad GCI = F_s \left| \frac{r^p [(U_{Medium} - U_{Fine})/U_H]}{1 - r^p} \right| \quad (3)$$

13 Where, U_{Medium} and U_{Fine} are the velocities obtained with the medium and fine
14 meshes, respectively. U_H is the time-average wind velocity at the height of the
15 building. The linear grid refinement factor, $r = \sqrt{2}$ in this case, while $p = 2$ is the
16 formal order of accuracy, corresponds to the second-order discretization schemes
17 used in the simulations. F_s is the safety factor, which is 1.25 when three or more
18 grids are considered.

19

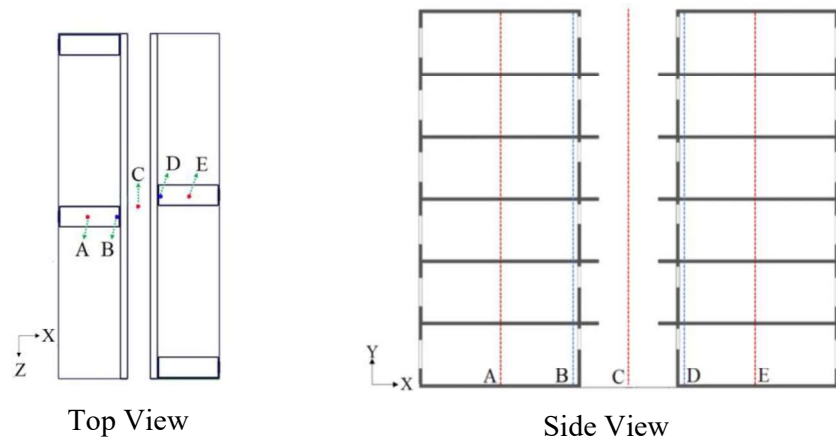


Figure 6. Locations of lines A, B, C, D, and E.

1

2 **Table 2.** Percentage difference of GCI values among different mesh sizes for
 3 lines A, B, C, D and E.

GCI Values	A	B	C	D	E	Average
Medium-Fine	0.62%	0.29%	1.40%	0.13%	0.30%	0.55%
Coarse-Fine	0.73%	0.43%	1.98%	0.30%	0.43%	0.77%

4

5 Figure 7 shows the vertical streamwise mean velocity (V_M) and pressure
 6 coefficient (C_p) profiles obtained with CFD using fine, medium, and coarse meshes.

7 The deviations of V_M (for lines A, C, and E) and deviations of C_p (for lines B and
 8 D) between medium-fine and coarse-fine meshes are presented in Table 2. In

9 general, the deviations are considered small, in between the range of 0.13%–1.98%.

10 For line C, the maximum average deviation of V_M is 1.98%, which is deemed
 11 acceptable, where large deviations occur mainly at the higher part of the building.

12 Meanwhile, the C_p for inlet and outlet rooms are measured on internal walls next
 13 to the void. As shown in Figure 7, there is no significant deviation between of C_p

14 between the medium-fine and coarse-fine meshes on lines B and D. It shows the
 15 grid sensitivity analysis showing good agreement, and the average normalized

1 deviation between the medium mesh and fine mesh is less than 0.55%. Therefore,
2 the medium mesh is selected for further analysis.

3 The quantitative metrics used for model verification are Root Mean Square
4 Error (RMSE) and Factor of two of observation (FAC2).

$$5 \quad RMSE = \sqrt{\frac{1}{n} \sum_{i=1}^n (P_i - Q_i)^2} \quad (4)$$

$$6 \quad FAC2 = \frac{1}{n} \sum_{i=1}^n N_i \quad (5)$$

$$7 \quad N_i = \begin{cases} 1 & \text{if } 0.5 \leq \frac{P_i}{O_i} \leq 2 \\ 0; & \text{otherwise} \end{cases} \quad (6)$$

8 Where, P_i is the value obtained from the reference grid, Q_i is the value obtained
9 from the RKE results published by Kumar et al. (2021). In the model verification
10 with Kumar et al.(2021), for the wind velocity of Line A,C, and E ,the RMSE
11 values are 0.057, 0.033 and 0.042 respectively. For the wind pressure of Line B
12 and D, the RMSE values are 0.194 and 0.127 respectively. The average of the
13 obtained RMSE values is 0.091, which is considered acceptable.

14 In the model verification with Kumar et al.(2021), for V_M of Line A, C, and E
15 ,the FAC2 values are 0.835, 0.86 and 0.725 respectively. For C_p of Line B and D,
16 the FAC2 values are 0.735 and 1.0 respectively. The average of the obtained FAC2
17 values is 0.831, indicating 83.1% of the data are within the acceptable range of
18 error. This is considered acceptable. As shown in Figure 7, the V_M and C_p profiles
19 by the reference grid (i.e., the medium mesh with 12,866,647 cells) are in good
20 agreement with Kumar et al.'s CFD and the wind tunnel results.

21

1 In this study, the values of U_H and A_o are 3.95 m/s and 0.00016m², respectively.
2 Higher DFR indicates the indoor air is purged at a higher rate, but it does not
3 indicate the air mixing within the building.

4 Air exchange efficiency (AEE) is used to study air mixing. It is used to quantify
5 the efficiency of the approaching flow to flush out a ventilated building (Hang &
6 Li, 2011), as defined by Equation (8) below:

$$7 \quad AEE = \frac{\bar{\tau}_r}{2\langle\tau_{av}\rangle} \times 100 [\%] \quad (8)$$

8 Where, $\bar{\tau}_r$ is the Age of Air (AOA) at the outlet opening and τ_{av} is the volume
9 average AOA in the building (van Hooff et al., 2013). However, AEE has a
10 fundamental limitation as it only quantifies the air distribution within a room based
11 on flow magnitude and profile. It measures the local mean AOA of the building
12 relative to its volume average AOA. A lower AEE is observed when there is a
13 higher variance between the local mean AOA and the volume average AOA, and
14 vice versa.

15 The AOA (φ) was obtained by solving the following steady-flow scalar
16 transport equation (Chanteloup & Mirade, 2009):

$$\nabla \cdot (\rho U \varphi) - \nabla \cdot (\Gamma \nabla \varphi) = 1 \quad (9)$$

17 The diffusion coefficient, Γ is calculated using Equation (10) (Chanteloup &
18 Mirade, 2009):

$$\Gamma = \rho D + \frac{\mu_t}{S_{c_t}} \quad (10)$$

19 Where, $D = 2.88 \times 10^{-5}$ m²/s is the laminar viscosity for air at the operating
20 temperature of 20°C, μ_t is the local turbulent viscosity, $S_{c_t}=0.7$ is the turbulent
21 Schmidt number. The transport equation was implemented in Fluent as UDS to
22 obtain the AOA distribution within the ventilated enclosures.

1 To quantify trade-off between AEE and DFR values, the optimal configuration
 2 that balances high DFR and high AEE should be obtained. Hence, the following
 3 objective function is proposed by Tai et al. (2022), to maximize the combinatorial
 4 effects of DFR and AEE:

$$5 \quad \alpha = DFR \times \left(\frac{AEE}{100} \right) \quad (11)$$

6 However, Equation (11) is only suitable when $AEE \leq 50\%$. For cases where
 7 AEE is larger than 50%, the α will also increase, leading to strong piston flow
 8 instead of the favorable perfect mixture of $AEE = 50\%$. Hence, the following
 9 objective function is proposed:

$$10 \quad \alpha = DFR \times \left(\frac{50 - |AEE - 50|}{100} \right) \quad (12)$$

11 The effect of a particular opening configuration n of block P on block Q can be
 12 quantified using the following equation:

$$\Delta X_n^P = \left(\frac{X_n^P}{\frac{1}{N} (\sum_{i=1}^N X_i^Q)} - 1 \right) \times 100\% \quad (13)$$

13 Where ΔX is the deviation of the performance metric X of block P from the
 14 average value of block Q, subscript i represent the i^{th} opening configurations
 15 block Q and N is the number of opening configurations of block Q.

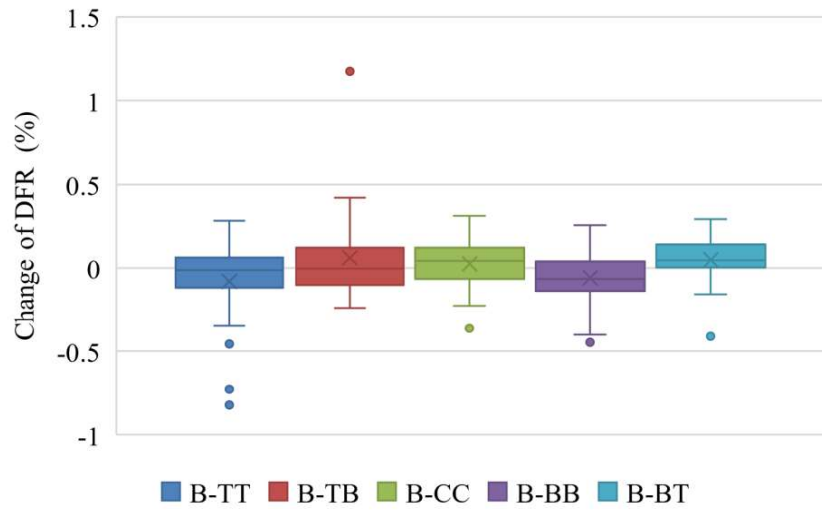
16

17 **3. Impact of opening configurations on block A**

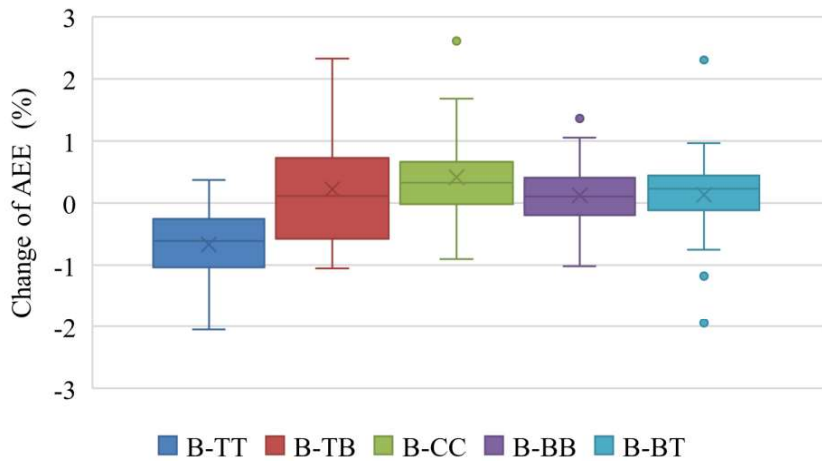
18 *3.1 Overall ventilation performance*

19 The impact of opening configurations in block B on the DFR and AEE in
 20 block A across various opening configurations is shown in Figures 8. The opening
 21 configurations in block B have no obvious impact on the DFR and AEE in the
 22 rooms in block A, fluctuating within $\pm 1.5\%$ and $\pm 3\%$ of the average values for

1 DFR and AEE, respectively, and with a mean value of approximately zero.
 2 Therefore, the AEE and DFR values for block A are the average values of the
 3 combination with five different block B's opening configurations.
 4



(a)



(b)

Figure 8. The impact of opening configurations of block B on (a) DFR, and (b) AEE of block A.

5

1 The ventilation performance of block A for various opening configurations is
2 presented in Table 3. On level 1, the best performance for both AEE and DFR is
3 produced by the A-TT and A-TB configurations, with the highest α value of 0.265
4 being registered. Their higher value is attributed to an AEE value closer to the
5 perfect mixture, which is approaching 50 %. On level 2, the largest α value is
6 possessed by the A-CC configuration. Followed by this is the A-TB configuration
7 with a higher α value. On level 3, the highest α is scored by the A-TB
8 configuration. This is due to their nearly perfect AEE and higher DFR values,
9 which create a solid balance between the two. In contrast, higher DFR values on
10 both levels 2 to 3 are demonstrated by the A-BB configuration, yet the lowest α
11 values among all configurations are scored by it due to its excessively low AEE
12 values, which are less than 40%.

13 For levels 4 to 6, the highest α value is scored by the A-BT configuration,
14 followed by the A-CC configuration on levels 4 to 5 and A-BB configuration on
15 level 6 with a higher α values. The worst α is scored by the A-TT configuration.
16 This is attributed to its low AEE values on levels 4 to 6, which is about 37%-40%.
17 Although its DFR value is the highest on level 4, there is little difference in DFR
18 values for different opening configurations in general. The AEE values of the A-
19 BT and A-CC configurations on levels 4 and 5 are close to the perfect mixing,
20 which are about 1 to 4% below or above the perfect mixture. The AEE and DFR
21 performance for the A-BT configuration is the best on level 6.

22 In summary, for optimal ventilation performance of block A, the recommended
23 opening configurations are the A-TT and A-TB for level 1, and the A-CC and A-
24 TB for level 2. The A-TB Configuration is deemed optimal for level 3. For levels
25 4 to 5, both A-BT and A-CC configurations are deemed optimal. For level 6, the

1 A-BT Configuration is regarded as optimal. Overall, it can be observed that A-TB
 2 configuration performs better in levels 1 to 3 and A-BT in levels 4 to 6.

3

4 **Table 3.** Ventilation performance of block A of different opening configuration.

Level	Ventilation Performance	A-TT	A-TB	A-CC	A-BB	A-BT
1	α	0.265	0.265	0.201	0.220	0.236
	DFR	0.535	0.536	0.535	0.560	0.532
	AEE	50.297	50.495	62.580	39.321	44.417
2	α	0.216	0.243	0.246	0.203	0.215
	DFR	0.530	0.535	0.531	0.551	0.517
	AEE	59.353	54.507	53.553	36.863	41.555
3	α	0.247	0.262	0.235	0.208	0.216
	DFR	0.541	0.539	0.536	0.556	0.523
	AEE	45.781	51.185	56.096	37.361	41.388
4	α	0.211	0.232	0.247	0.230	0.248
	DFR	0.556	0.531	0.536	0.553	0.536
	AEE	38.023	43.515	53.841	41.702	46.243
5	α	0.197	0.215	0.255	0.211	0.255
	DFR	0.526	0.507	0.522	0.529	0.534
	AEE	37.491	42.422	48.732	60.103	52.180
6	α	0.170	0.180	0.207	0.219	0.240
	DFR	0.433	0.418	0.462	0.483	0.496
	AEE	39.353	43.228	44.897	54.670	48.228
Color scale		Min				Max

5

6 3.2 Indoor airflow characteristic

7 Similar to DFR performance, the variation of the indoor air velocity profiles in
 8 block A at line A is less than $\pm 0.5\%$ by varying block B's opening configurations.

9 Therefore, five opening configurations of block A in combination with the B-TT
 10 configuration have been selected to represent the effect of block A's opening
 11 configurations on block A itself, to simplify the analysis.

1 3.2.1 Velocity profile (V_M/U_H)

2 Indoor air velocity profiles, V_M/U_H , at line A was measured to investigate how
3 the efficiency of natural ventilation for block A might be improved by the openings
4 positions, as shown in Figure 9(a).

5

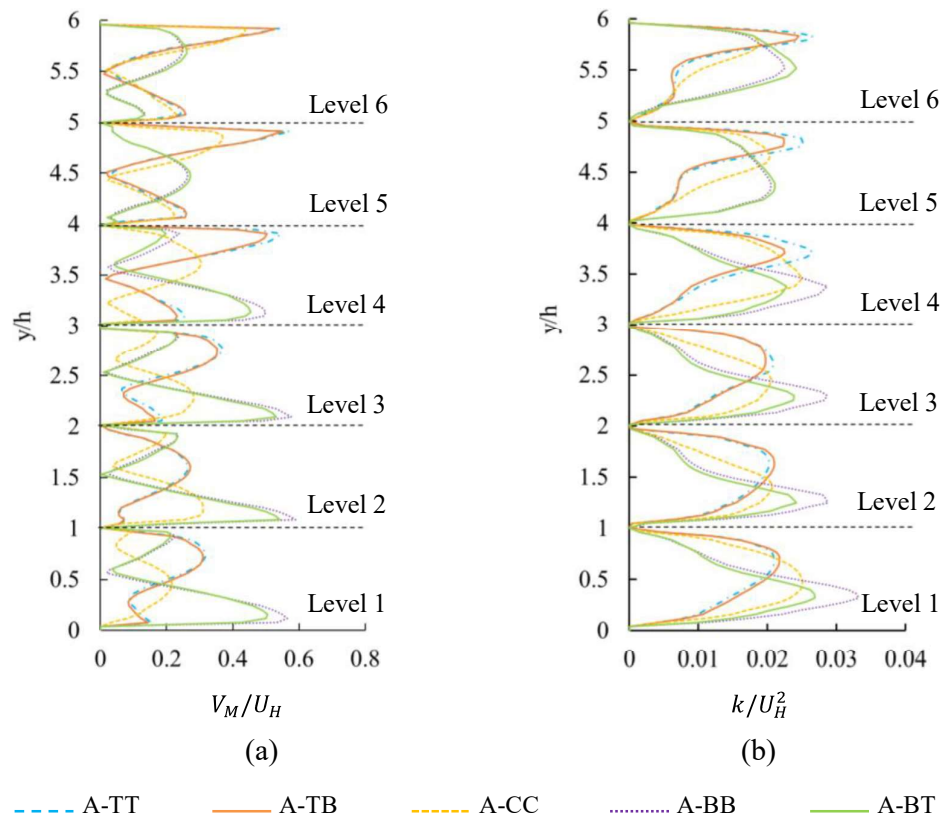


Figure 9. V_M/U_H profile (a) and TKE profile (b) at line A for block A with various opening configurations

6

7 The impact of block A with various opening configurations on V_M/U_H in block
8 A is illustrated in Figure 9(a). On levels 1 to 3, the best performance is shown by
9 the A-BB and A-BT configurations, with peaks between 0.50-0.60. On level 4,
10 maximum V_M/U_H values produced by the top and bottom openings are found to
11 be similar and exceeded those generated by the A-CC configurations. On levels 5

1 and 6, A-TT and A-TB configurations are distinguished, showing peaks between
2 0.53-0.58. It is observed that the V_M/U_H behavior remained largely consistent
3 when the outlet position is altered, while the inlet position is kept steady. This
4 observation indicates that a more significant impact on V_M/U_H is exerted by the
5 inlet opening position than the outlet position.

6 Differing maximum V_M/U_H values across levels are identified for block A.
7 When the inlet opening is positioned at the bottom, these values are concentrated
8 in the lower part of the room from levels 1 to 4, migrated to the middle of the room
9 at level 5, and moved to the upper section at level 6. In contrast, with the top inlet,
10 peak V_M/U_H values are found in the middle and upper sections of the room from
11 levels 1 to 3 and are located near the roof from levels 4 to 6. With a centered inlet,
12 the peak V_M/U_H is situated in the middle of the room at level 1, descended to the
13 lower part on levels 2 and 3, and is seen to ascend to the upper region from levels
14 4 to 6, eventually appearing close to the roof. It is noteworthy that on levels 5 and
15 6, a trend towards the upper part of the room is seen for the maximum V_M/U_H
16 values of all opening combinations.

17 In general, the position of the inlet exerts a more significant influence on V_M/U_H
18 than the outlet, consistent with the findings by Li et al. (2023). For block A, the
19 bottom inlet is optimal on levels 1 to 3, levels 4 witnesses comparable results
20 between top and bottom inlets (with both outperforming the center inlet), and an
21 advantage is seen for the top inlet on levels 5 and 6.

22 3.2.2 *Indoor airflow*

23 In the previous analysis, it was observed that different opening configurations
24 with the same inlet opening position were performed similarly for rooms located
25 in the middle of the building. To simplify the illustration, 5 out of 25 cases with

1 different combinations of opening configurations for block A were chosen to
2 analyze their velocity vectors, as shown in Figures 10.

3 The Coanda effect is prominent in A-TT configuration, especially from level 3
4 onwards, as depicted in Figures 10(a). This effect results in the jets adhering
5 closely to the ceilings, accompanied by a noticeable rise in flow velocities. On
6 levels 4 to 6, short circuit flows are observed, resulting in low AEE in the 3 levels.

7 For the A-TB configuration as shown in Figure 10(b), the Coanda effect is
8 noticeable on levels 4 to 6. The jets enter the top inlet openings and adhere to the
9 ceilings and leeward walls before exiting the outlet openings at the bottom. On
10 levels 1 to 3, the jets detach from the ceilings near the center of the rooms and are
11 directed to the outlet openings. Flow circulation zones are observed between the
12 jets and the floors, resulting in near perfect mixing (near 50% AEE) on levels 1 to
13 3.

14 Presented in Figure 10(c) is the velocity vector for A-CC. The Piston effect is
15 prominent on levels 1 and 4, resulting in high AEE. On levels 2 and 3, the jets are
16 directed towards the floors before exiting the leeward openings. A circulation zone
17 is observed between the ceiling and windward wall in both rooms, resulting in a
18 near perfect mixture in both rooms. Conversely, the jets are directed towards the
19 ceiling on levels 5 and 6, with a circulation zone observed between the windward
20 wall and the floor in each room. Stronger circulation is observed on level 5,
21 resulting in near perfect mixing (AEE = 48.75%), compared to level 6 (AEE =
22 44.86%).

23 Figures 10(d) highlight the A-BB configurations. The jets adhere to the floors
24 on levels 1 to 4, where the Coanda effect drives the jets through the room's lower
25 section and creating short circuit flows. This results in low AEE (below 42%). On

1 levels 5 and 6 display a distinct pattern dominated by the Piston effect, with jets
2 directing towards the ceilings from the bottom inlet openings before exiting the
3 leeward opening at the bottom, resulting in high AEE values.

4 Figure 10(e) shows the velocity vector of A-BT. The jet of each room is attached
5 to the floor from the bottom inlet opening and exits the top opening at the leeward
6 wall. A circulation zone is observed between the jet and the ceiling. However, the
7 low AEE values show that the flow behaves more like a short circuit flow. On
8 levels 5 and 6, the jets are directed towards the ceiling from the bottom inlet
9 openings before exiting the top outlet openings. The AEE values for both levels 5
10 and 6 (52.37% and 47.96%) show that the flow is a near perfect mixture.

11

12

13

14

15

16

17

18

19

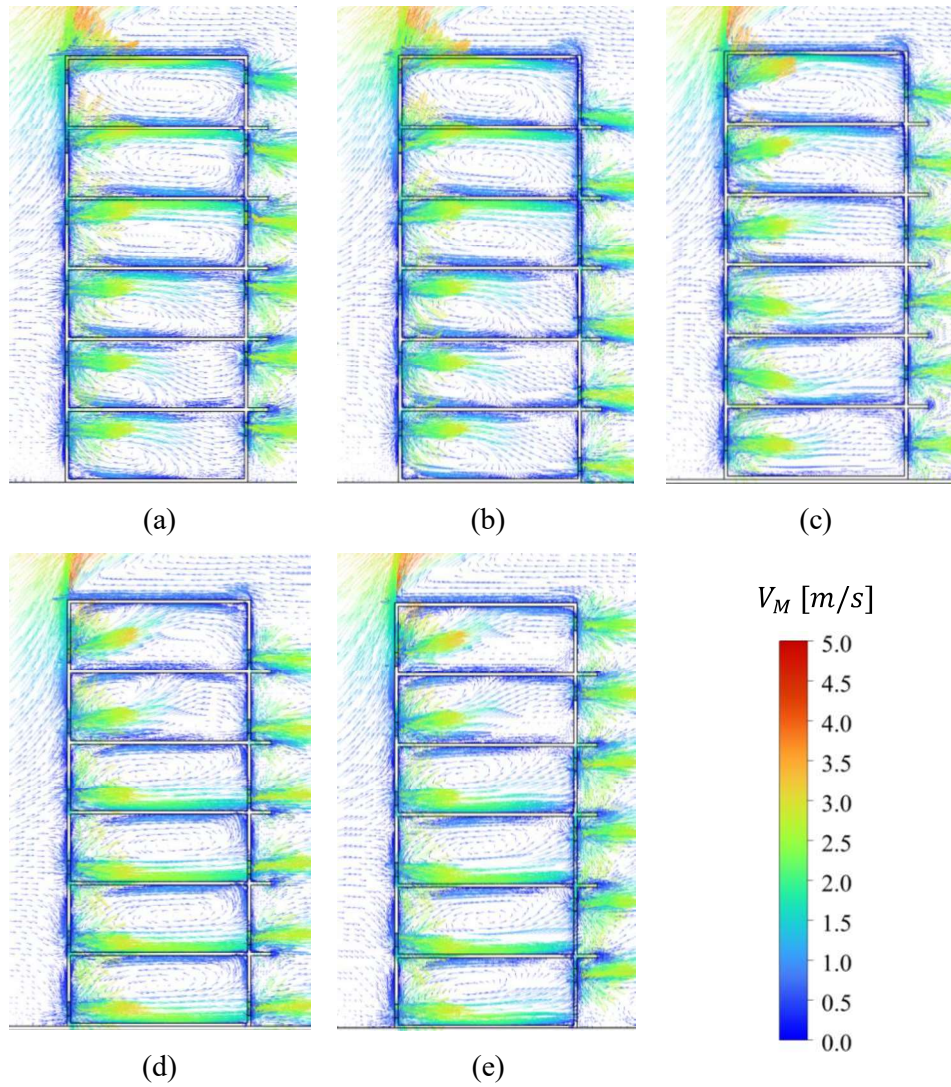


Figure 10. Velocity vectors for (a) A-TT, (b) A-TB, (c) A-CC, (d) A-BB, and (e) A-BT.

1

2 3.2.3 TKE profile (k/U_H^2)

3 Figure 9(b) illustrates the TKE profile (k/U_H^2) of the building at lines A for
 4 block A. The TKE profile for the different opening configurations varies
 5 significantly on each level. On levels 1 to 3, the TKE values for A-BB/B-TT and
 6 A-BT/B-TT configurations are higher compared to other configurations. It is
 7 noteworthy that the A-BB/B-TT configuration has the largest TKE magnitude on
 8 levels 1 to 4, while the A-TT/B-TT configuration has the largest TKE magnitude

1 on levels 5 and 6. The TKE magnitude for A-BB decreases gradually from the
2 largest to the lowest among all configurations from levels 1 to 6, while the opposite
3 is true for A-TT.

4 The TKE profile for A-TB is nearly identical to the TKE profile of A-TT. On
5 levels 1 to 3, the TKE magnitude of configurations are nearly identical. However,
6 the TKE magnitudes of A-TB on levels 4 to 6 are about 7.8% – 15.2% lower than
7 A-TT. This observation is in line with Figures 10(a) and (b), where the circulation
8 zones for A-TT are larger than A-TB on levels 4 to 6, thereby introducing more
9 TKE into the flow, while the circulation zones for both configurations on levels 1
10 to 3 are nearly identical.

11 The TKE profile for A-BT is also nearly identical to A-BB, but lower in
12 magnitude on levels 1 to 4. This is attributed to larger circulation zones that occur
13 in A-BB, between the jets and the ceilings (see Figure 10(d)), which introduce
14 more TKE into the flow. On levels 5 and 6, the size of the circulation zones for
15 both configurations are nearly identical (see also Figure 10(e)), therefore the TKE
16 profiles are nearly identical.

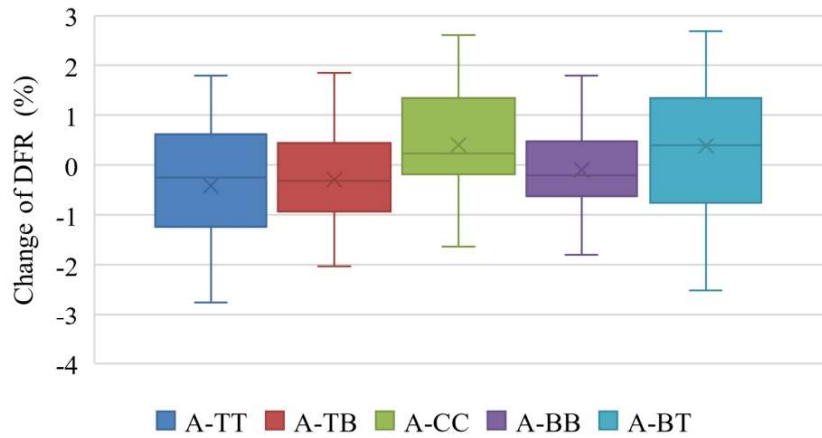
17

18 **4. Impact of opening configurations on block B**

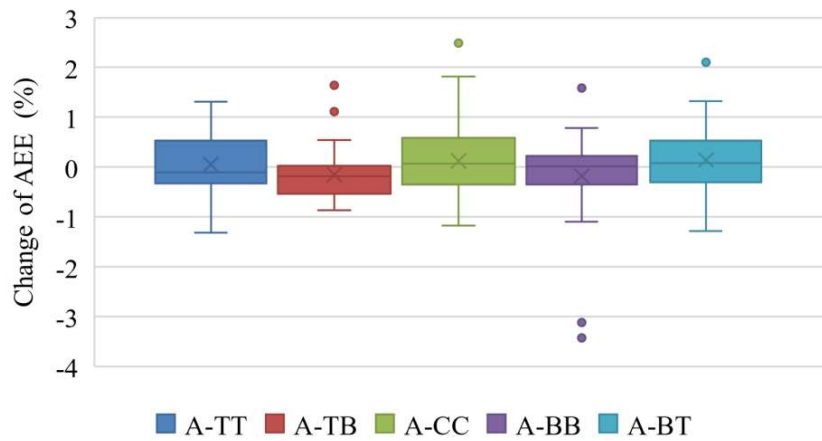
19 *4.1 Overall ventilation performance*

20 The impact of opening configurations in block A on the DFR and AEE in block
21 B across various opening configurations is presented in Figures 11, computed
22 using Equation (13). The opening configurations in block A have no obvious
23 impact on the DFR and AEE in the rooms in block B, fluctuating within $\pm 3.5\%$ of
24 the average values for both DFR and AEE, with a mean value of approximately
25 zero. Therefore, the AEE and DFR values for block B are the average values of
26 the combination with five different block A's opening configurations.

1



(a)



(b)

Figure 11. The impact of opening configurations of block A on (a) DFR, and (b) AEE of block B.

2

3 The ventilation performance of block B for various opening configurations is
4 presented in Table 4. On level 1, the best performance for both AEE and DFR is
5 produced by the B-TT configuration, with the highest α value of 0.131 being
6 registered. On level 2, the largest α value is possessed by the B-TB configuration;
7 however, a divergence in its AEE and DFR performances is observed. Specifically,
8 an AEE value approaching 50% is seen, while the DFR value is found to be the

1 lowest compared to other configurations. Followed by this is the B-BB
2 configuration with a higher α value; its higher value is attributed to an AEE value
3 closer to the perfect mixture and a high DFR value. In contrast, higher DFR values
4 on both levels 1 and 2 are demonstrated by the B-CC configuration, yet the lowest
5 α values among all configurations are scored by it due to its excessive AEE values,
6 which are found to exceed 60%.

7 For levels 3 to 6, when compared to the B-TT, B-TB, and B-CC configurations,
8 lower α values are scored by the B-BB and B-BT configurations. The worst α is
9 scored by the B-BB configuration. This is attributed to its high AEE performance,
10 which is about 66%-69%. However, its DFR values are observed to be only
11 marginally higher than those of the B-TT, B-TB, and B-CC configurations in
12 general. Both the B-TB and B-CC configurations demonstrate better performance
13 on α than the B-TT configuration, with their α scores being quite similar. The B-
14 TT configuration has AEE values close to 50%, which are about 1 to 2% below
15 the perfect mixture. However, it also has the lowest DFR values when compared
16 to all other configurations. The B-CC configuration, on the other hand, has a DFR
17 higher than both the B-TT and B-TB configurations, even though its AEE is 4-6%
18 above the perfect mixture. In conclusion, the α scores for the B-TB and B-CC
19 configurations are about 32%-42% higher than those of the B-BB configuration.

20 In summary, for optimal ventilation performance of block B, the recommended
21 opening configurations are the B-TT for level 1, and the B-TB for level 2. For
22 levels 3 to 6, the B-TB, and B-CC configurations both are deemed optimal. The
23 findings indicate that a one-configuration-fits-all approach may not be suitable in
24 sheltered urban buildings, which is more recurring in nowadays dense urban
25 landscapes.

1

2 **Table 4.** Ventilation performance of block B of different opening configuration.

Level	Ventilation Performance	B-TT	B-TB	B-CC	B-BB	B-BT
1	α (-)	0.131	0.116	0.094	0.109	0.113
	DFR (-)	0.266	0.261	0.264	0.251	0.256
	AEE (%)	50.775	55.643	64.478	43.525	44.157
2	α (-)	0.111	0.122	0.103	0.119	0.112
	DFR (-)	0.256	0.253	0.263	0.259	0.262
	AEE (%)	43.168	48.106	60.810	54.145	57.414
3	α (-)	0.103	0.110	0.109	0.083	0.091
	DFR (-)	0.240	0.233	0.248	0.249	0.251
	AEE (%)	43.031	47.387	56.324	66.524	63.908
4	α (-)	0.097	0.102	0.102	0.072	0.086
	DFR (-)	0.221	0.213	0.227	0.228	0.232
	AEE (%)	43.636	47.651	55.302	68.648	62.858
5	α (-)	0.090	0.093	0.092	0.067	0.083
	DFR (-)	0.202	0.193	0.206	0.206	0.212
	AEE (%)	44.218	48.079	55.081	67.565	60.838
6	α (-)	0.080	0.084	0.085	0.064	0.078
	DFR (-)	0.180	0.173	0.187	0.189	0.193
	AEE (%)	44.299	48.177	54.594	66.105	59.602
Color scale		Min				Max

3

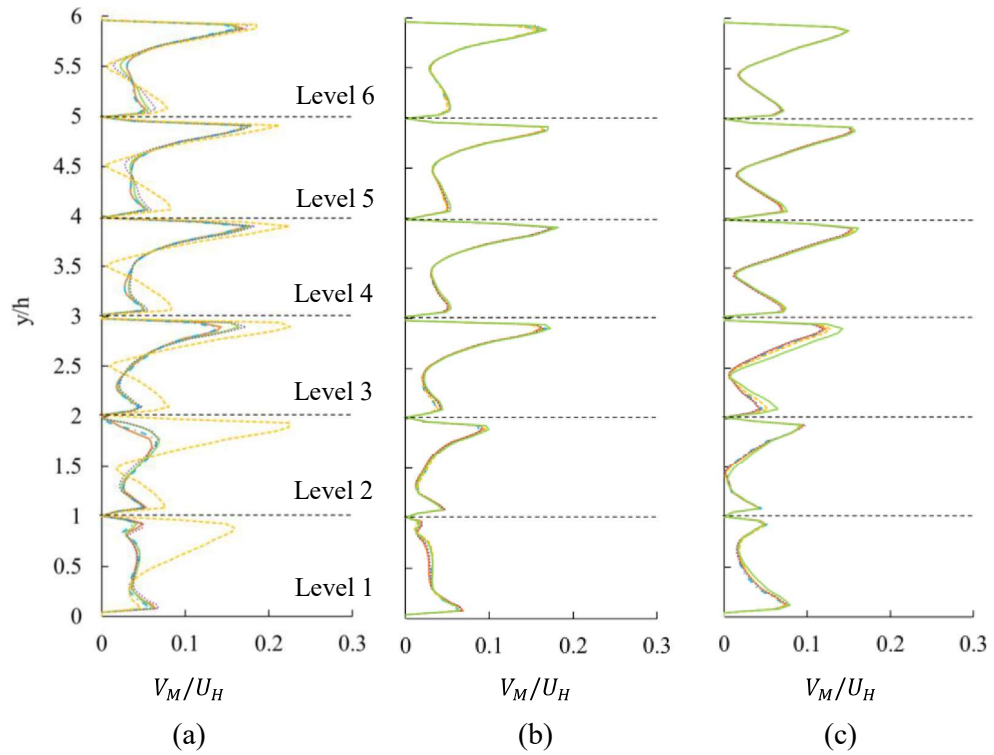
1 4.2 Indoor airflow characteristic

2 4.2.1 Velocity profile (V_M/U_H)

3 The insights into the V_M/U_H for block B under various opening configurations
4 influenced by different opening configurations of block A, are presented in Figures
5 12(a) through (e). At line E, it is noted that the V_M/U_H peak for the A-CC/B-TT
6 case is the highest among the 25 cases, with an average of 0.21 (see Figure 12(a)).
7 For block B with top-top and top-bottom configurations, the average peak V_M/U_H
8 values on levels 2 to 6 are around 0.17 and 0.16, respectively, surpassing the other
9 three configurations, as shown in Figures 12(a) and (b). A consistent pattern is
10 exhibited by the V_M/U_H for block B with B-TT and B-TB configurations across
11 levels—levels 1 and 2 have a lower V_M/U_H , and a mark increase in V_M/U_H is seen
12 on levels 3 to 6, improving by about 30-60%. When examining the V_M/U_H for
13 block B with diverse opening combinations (as shown in Figures 12(a) through
14 (d)), distinct patterns are identified: top inlet configurations exhibit lower V_M/U_H
15 on level 1 but show increased values on levels 2 to 6. In contrast, configurations
16 with bottom inlets are more prominent on level 1 and decline from levels 2 to 6.
17 The V_M/U_H of the B-CC configuration is generally found to lie between those of
18 the top and bottom inlets. Additionally, it is observed that symmetrical inlet and
19 outlet configurations slightly outperformed their asymmetrical counterparts.

20 A shared pattern is observed for all opening configurations of block B: from
21 levels 2 to 6, maximum V_M/U_H values approach the roof of the room, while on
22 level 1, they are observed to be closer to the room's floor, with the A-CC/B-TT
23 configuration being the sole exception.

1 Like block A, the position of the inlet exerted a more significant influence on
2 V_M/U_H than the outlet for block B. The A-CC/B-TT opening combination
3 consistently show the best V_M/U_H performance among all configurations.
4



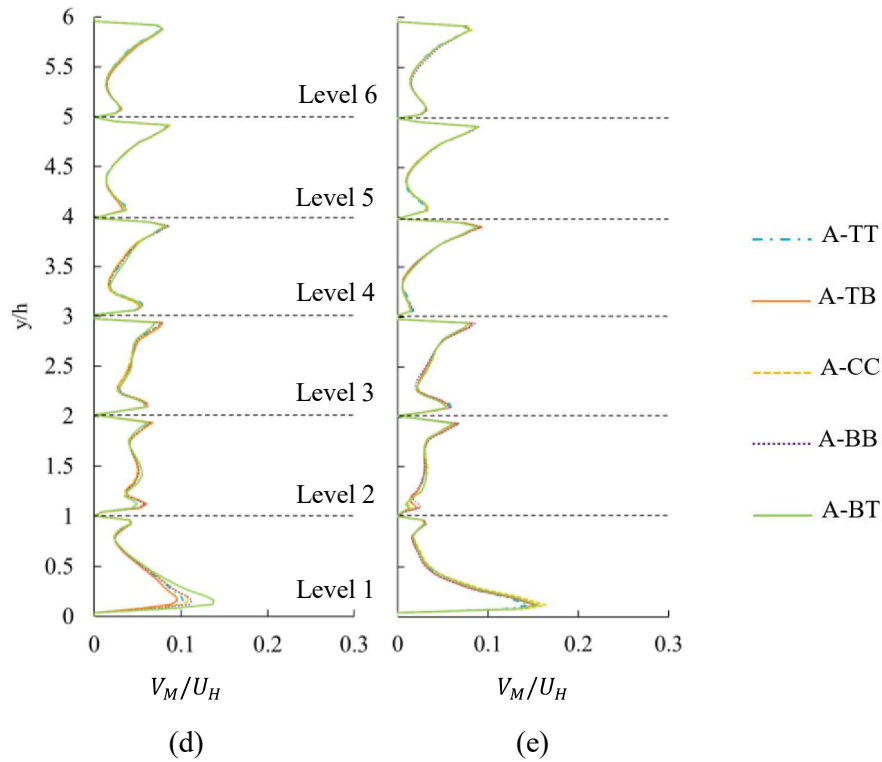


Figure 12. V_M/U_H profiles at line E for block B with (a) B-TT, (b) B-TB, (c) B-CC, (d) B-BB, and (e) B-BT configurations.

1

2 4.2.2 Indoor airflow

3 The analysis in Section 4.2.1 showed that block A of different opening
 4 configurations do not give significant impact to the velocity profiles of each
 5 opening configuration in block B, except for B-TT where the impact of A-CC is
 6 prominent (see Figure 12(a)). To simplify the illustration, 6 out of 25 cases with
 7 different combinations of opening configurations are chosen to analyze their
 8 velocity vectors, as shown in Figure 13. Due to the negative wind pressure area
 9 generated above the roof and leeward side of the building, fresh air enters block B
 10 from the opening at the leeward side. Therefore, the wind direction is opposite to
 11 block A. This is consistent with the results by Kumar et al. (2021).

12 Figures 13(a) to (c) show the velocity vectors for configurations A-TT/B-TT,
 13 A-CC/B-TT, and A-TB/B-TB. Note that the velocity vectors for A-TT/B-TT and

1 A-TB/B-TB are nearly identical in the first half of the building, due to the top
2 opening in block B. The jets enter the top inlet openings at about the same velocity
3 and lose momentum at about the same positions in both configurations. However,
4 due to the different positions of the outlet openings, different flow behaviors are
5 produced by the two configurations. For the A-TT/B-TT configuration, due to the
6 outlet openings being placed in line with the flow direction from the inlet openings,
7 the flow behaves more like a short circuit flow, with the average AEE of lower
8 than 45% for levels 2 to 6. The AEE for level 1 is a near perfect mixture. For the
9 B-TB configurations where the outlet openings are place diagonally to the top inlet
10 openings, making the $\bar{\tau}_r$ of the flow at the outlet openings are higher than the B-
11 TT configurations, resulting in higher AEE the B-TT configurations in general.
12 On level 1, the B-TB's flow behaves more like a piston flow, with AEE of 55.64%.

13 On levels 2 to 6, the jets enter through the top inlet openings, adhere to the
14 ceilings, then detach around the center of rooms before exiting through the bottom
15 outlet openings. Flow circulation zones between jets and the floors are noticed,
16 resulting in AEE values of 47% to 48%.

17 Compared to other B-TT opening configurations (see Figure 13(a)), the A-
18 CC/B-TT configuration has higher velocities and momentum in the center of
19 rooms, as shown in Figure 13(b). This is consistent with the V_M/U_H profiles
20 presented in Figure 12(a), where the peak velocity for A-CC/B-TT is higher than
21 the other B-TT configurations. In general, the airflow behavior of the A-CC/B-TT
22 configuration is generally similar to that of the A-TT/B-TT configuration, as the
23 opening configurations of block A affect only $\pm 2.5\%$ of the AEE values for all
24 the B-TT configurations.

1 Like the top inlet configuration, the bottom inlet configurations exhibit nearly
2 identical velocity vectors in the front half of the rooms and lose momentum at
3 similar locations, as depicted in Figures 13(d) and (e). On levels 1 and 2, the jets
4 are directed towards the floors. On level 1, the outlet opening of the B-BB
5 configuration is aligned with the inlet opening, resulting in a short circuit flow,
6 while the B-BT's outlet opening is located diagonally to the inlet opening,
7 resulting in higher AEE value than the B-BB configuration. However, the level 1's
8 AEE values for both B-BB and B-BT are below 45%. The airflows for B-BB and
9 B-BT configurations on level 2 behave more like piston flows, with AEE values
10 of 54.15% and 57.41%, respectively. On levels 3 to 6, the jets are directed towards
11 the ceilings before exiting the outlet openings under the influence of the Coanda
12 effect. However, the outlet openings of the B-BT configuration are in line with the
13 airflow directions, resulting in lower $\bar{\tau}_r$ and AEE values compared to the B-BB
14 configuration. The flows for B-BT configuration on levels 3 to 6 behave like piston
15 flows, with AEE values ranging from 66.11% to 68.65%.

16 Figure 13(f) presents the velocity vector for the A-CC/B-CC configuration. On
17 level 1, the alignment of the inlet and outlet positions results in a piston effect,
18 producing a high AEE of 64.48%. The Coanda effect is observed on levels 2 to 6,
19 where the jets move towards and flow along the ceiling from the inlet openings,
20 before exiting through the center outlet openings. The flows gain momentum as
21 the room level increases, result in a shorter $\bar{\tau}_r$ and lower AEE values at higher
22 levels. The AEE gradually decreases from 60.081% on level 2 to 54.594% on level
23 6.

24

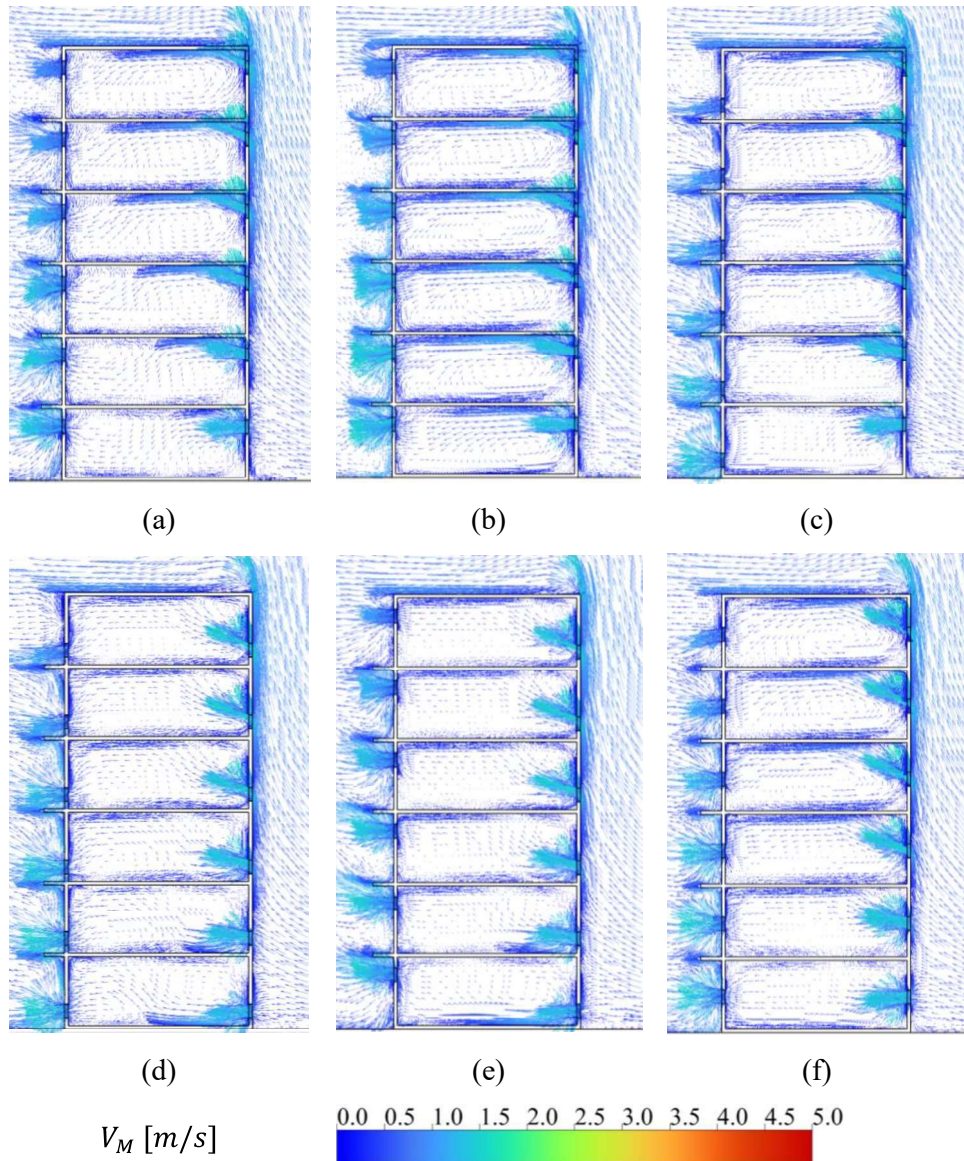


Figure 13. Velocity vectors for (a) A-TT/B-TT, (b) A-CC/B-TT, (c) A-TB/B-TB, (d) A-BB/B-BB, (e) A-BT/B-BT, and (f) A-CC/B-CC.

1

2 4.2.3 TKE profile (k/U_H^2)

3 For block B, it can be observed that changing the opening configurations of
 4 block A has no significant effect on the TKE, except for the A-CC/B-TT
 5 configuration, as shown in Figures 14(a) to (d). Note that the TKE magnitude for
 6 A-CC/B-TT on each level is also the largest among all the opening configurations,
 7 about 15% to 40% higher than the average TKE magnitude of all other opening

1 configurations of block A/B-TT. Figure 15 shows the TKE contour for block B.
2 Comparison of Figure 15(a) and (b) confirms the TKE for A-CC/B-TT is higher.
3 A closer examination of Figure 13 reveals a visible circulation zone on each level
4 between the jet and the floor for the A-CC/B-TT configuration, which introduces
5 TKE to the flow.

6 The block B TKE profiles measured at the middle of the rooms with the same
7 inlet positions, i.e., B-TT and B-TB or B-BB and B-BT configurations, exhibit
8 similar patterns. This is due to the inlet flows possessing the same TKE from the
9 similar opening positions. However, their TKE magnitudes changes due to the
10 different outlet opening positions. This can be observed by comparing Figures 15(a)
11 and (c) for B-TT and B-TB, and Figures 15(d) and (e) for B-BB and B-BT, where
12 the TKE contours in the 2nd half of the rooms in both top-inlet and bottom-inlet
13 configurations are different.

14 The impact of outlet opening positions on the TKE for B-TT and B-TB is
15 complex. On levels 1 and 2, the TKE magnitudes for B-TB are 1.25% and 3.85%
16 lower than those for B-TT, respectively. In contrast, the TKE magnitudes for B-
17 TB are about 2% higher than those for B-TT on levels 3 and 4, and 4.2% higher
18 on level 6. On level 5, the difference is insignificant.

19 Conversely, the influence of the outlet opening positions on the TKE for B-BB
20 and B-BT is straight forward. The TKE magnitudes for B-BT are higher than those
21 for B-BB on all levels except level 3. On levels 1 and 2, the TKE magnitudes are
22 10.3% and 6.7% higher than those for B-BB, respectively. On level 3, the
23 difference in TKE magnitude is minor, approximately 0.7% lower than the B-BB
24 configuration. From level 4 to 6, the TKE magnitude for B-BT gradually increases

1 from 2.2% to 5.1% higher than that for B-BB. In general, the findings indicate that
2 the top outlet opening position can increase the TKE of the indoor airflow.

3 For the B-CC configuration, its TKE magnitudes consistently fall between B-
4 TT and B-BB on all levels 2 to 6 and are lower than those for B-TT and B-BB on
5 level 1. However, without considering the A-CC/B-TT configuration, TKE
6 magnitudes for all B-CC configurations are in between the B-TT and B-BB
7 configurations on levels 1, 2 and 6, and are higher than those for B-TT and B-BB
8 on levels 3 to 5. Figure 15(f) reveals that the indoor TKE distribution on all levels
9 for B-CC configuration are similar, which explains the seemingly consistent
10 magnitude of its TKE profile depicted in Figure 14(c).

11

12

13

14

15

16

17

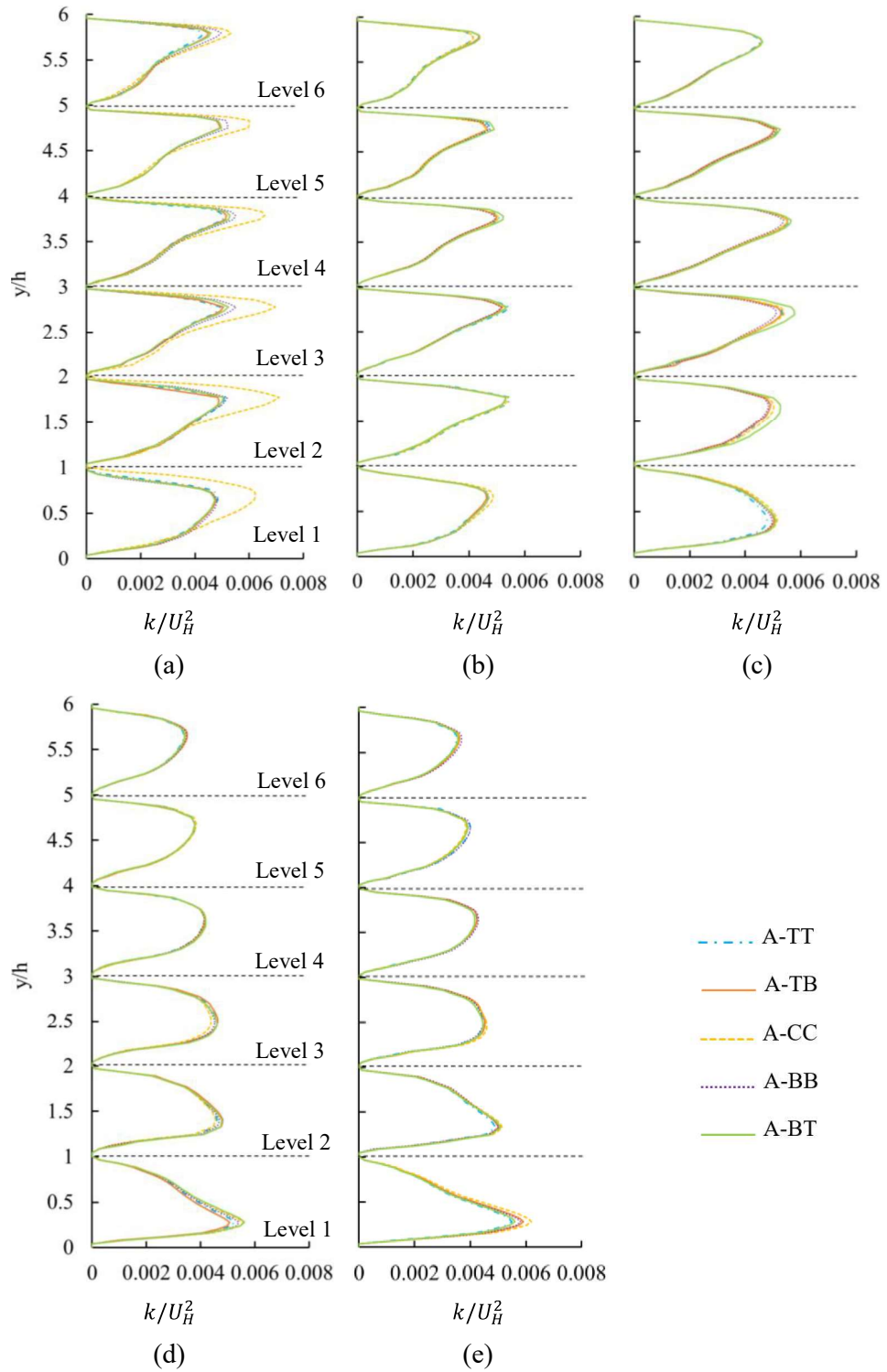


Figure 14. TKE profiles at line E in block B with (a) B-TT, (b) B-TB, (c) B-CC, (d) B-BB, and (e) B-BT configurations.

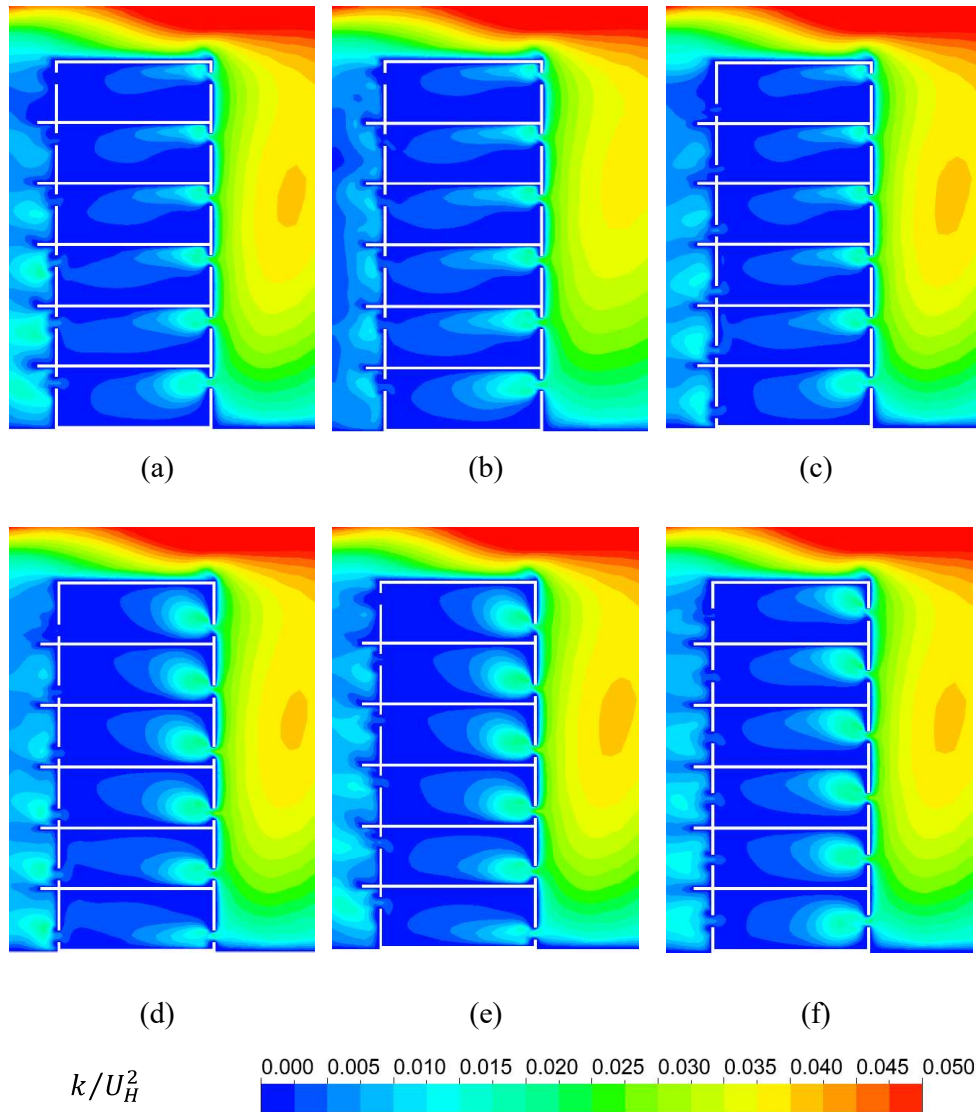


Figure 15. Selected k/U_H^2 contours for block B. (a) A-TT/B-TT, (b) A-CC/B-TT, (c) A-TB/B-TB, (d) A-BB/B-BB, (e) A-BT/B-BT, and (f) A-CC/B-CC.

1

2 **5. Discussion**

3 *5.1 Impact of opening configurations on block A*

4 The opening configurations in block B had negligible impact on the DFR and
 5 AEE in the rooms in block A. fluctuating within $\pm 1.5\%$ and $\pm 3\%$ of their averages,
 6 respectively. Considering both DFR and AEE, the top inlet configurations (A-TT
 7 and A-TB) recorded the highest α scores for level 1. Levels 2 showed optimal

1 performance from A-TB and A-CC, with the former maintaining the top α value
2 for level 3. Levels 4 and 5 presented closely matched α scores for A-CC and A-
3 BT. A-BT had the highest α score for level 6 at 0.240. Thus, generally, A-TB is
4 preferable for level 1 through 3, while A-BT presents consistent performance for
5 levels 4 through 6.

6 The position of the inlet had a greater influence on V_M/U_H than the outlet. The
7 bottom inlet is optimal on levels 1 through 3, V_M/U_H peaking at 0.50-0.60. Levels
8 4 show comparable results between the top and bottom inlets (with both
9 outperforming the middle inlet), and levels 5 and 6 show an advantage for the top
10 inlet, with the V_M/U_H magnitudes of 0.53-0.58.

11 The TKE was the highest with the A-BB configuration on the lower levels of
12 block A but declined on upper levels, whereas the TKE for A-TT was seen to
13 increase on upper levels. A-TB had a similar TKE to A-TT on lower levels but
14 was between 7.8% – 15.2% lower on the upper levels, indicating TKE's sensitivity
15 to specific configurations.

16

17 5.2 *Impact of opening configurations on block B*

18 The impact on block B by block A's opening configurations was minimal, with
19 DFR and AEE variations within $\pm 3.5\%$ of their averages. B-TT excelled at level
20 1, achieving the highest α score. At level 2, B-TB had the highest α score, despite
21 registering the lowest DFR, followed by B-BB with a slightly lower α score but
22 with higher AEE and DFR values. B-CC was less effective on levels 1 and 2. For
23 levels 3 to 6, the top and center inlet configurations (B-TT, B-TB, and B-CC)
24 outperformed the bottom inlet configurations (B-BB and B-BT). Compared to the

1 lowest α score for B-BB, those for B-TB and B-CC were 32-42% higher,
2 indicating a more favorable performance.

3 Like block A, the position of the inlet exerted a more significant influence on
4 V_M/U_H than the outlet for block B. The A-CC/B-TT opening combination
5 consistently demonstrated the best V_M/U_H performance among all configurations,
6 with an average of 0.21. There are distinctive patterns were identified: top inlet
7 configurations displayed lower V_M/U_H on level 1 but showed increased values on
8 levels 2 through 6. In contrast, the bottom inlet configurations were more
9 pronounced on level 1 and decreased from levels 2 to 6. The V_M/U_H of the B-CC
10 configuration was generally between those of the top and bottom inlets.

11 The influence of the opening configurations of block A on block B's indoor
12 airflow was negligible, except when A-CC is combined with B-TT, resulted in
13 significant variations in the indoor velocity profiles on all levels. Nevertheless, the
14 A-CC/B-TT configuration affected the AEE by only $\pm 2.5\%$ when compared with
15 other B-TT configurations. The same inlet configurations (such as A-TT/B-TT and
16 A-TB/B-TB) configurations behaved similarly at the front half of the rooms in
17 block B, but the flow behavior differed in the rear half due to the varied placement
18 of the outlet openings.

19 Block A's configurations also have a minimal impact on block B's TKE (within
20 $\pm 6\%$), except for the A-CC/B-TT combination, which experienced up to a 40%
21 increase compared to the average TKE of all combinations of block A with B-TT
22 configurations on level 2. This indicates that specific configuration pairings can
23 have a notable effect on airflow dynamics between blocks.

24

1 5.3 *Limitations and suggestions for future work*

2 The present study considers only steady wind in the direction normal to the inlet
3 openings. In real-world scenarios, the wind is unsteady and most of the time the
4 buildings are not built to face the wind perpendicularly. Therefore, it is suggested
5 to consider the wind from directions and transient wind in future studies.

6 The opening has multiple uses, including daylighting, ventilation, and views. In
7 real design scenarios, a more comprehensive configuration design is needed to
8 make it more practical, such as the size and number of openings, the dimension of
9 the void, impact of internal furniture, and wall partitions.

10 The results presented in this study are based on the window-to-wall ratio of
11 10.16% for each unit. Varying the window-to-wall ratio will alter the indoor
12 ventilation performance of the building. Therefore, further study under varying
13 window-to-wall ratio shall be considered.

14 Only the central units with openings are discussed in this study. Therefore,
15 whether fenestration performance would be consistent if other openings were
16 present next to the units is not known. Therefore, the study on the building model
17 with increased number of units with opening is required for future studies.

18 Furthermore, the current study is exclusively concentrated on wind-driven
19 ventilation, neglecting the impact of buoyancy forces and the interplay between
20 solar radiation and the design of openings. However, in practical applications,
21 these elements are crucial for achieving thermal comfort. Further research is
22 required in ensuring thermal comfort and optimizing energy use of buildings.

23

1 **6. Conclusions**

2 In this study, the ventilation performance of a double-loaded six-level apartment
3 building was analyzed through CFD simulations. The main objective was to
4 understand the influence of opening configurations on the natural cross ventilation
5 performance of windward and leeward blocks of the multi-level apartment. The
6 findings indicate that AEE, DFR, and TKE exhibit consistent patterns and specific
7 responses based on the level and configuration, highlighting the necessity for
8 tailored design choices for each building segment. Given the small variations of
9 AEE, DFR, and TKE for block B and minimal inter-block influences, the opening
10 configurations can be optimized within each block with limited impact on adjacent
11 structures. The findings call for a nuanced approach in building design to achieve
12 the desired airflow characteristics for a given environment. This work contributes
13 to a better understanding of ventilation phenomena in high-rise buildings, paving
14 the way for more sustainable urban environments.

15

16 **Acknowledgement:**

17 The project is funded by the Ministry of Higher Education Malaysia, under the
18 Fundamental Research Grant Scheme (FRGS Grant No.
19 FRGS/1/2023/TK08/SEGI/02/1).

20

1 **7. References:**

- 2 [1] ANSYS. (2020). *ANSYS Fluent Mosaic Technology Automatically Combines*
3 *Disparate Meshes with Polyhedral Elements for Fast, Accurate Flow*
4 *Resolution [White Paper]. ANSYS Inc.*
- 5 [2] Asfour, O. S. (2010). *Prediction of wind environment in different grouping*
6 *patterns of housing blocks. Energy and Buildings, 42(11), 2061–2069.*
7 *<https://doi.org/10.1016/j.enbuild.2010.06.015>*
- 8 [3] Bangalee, M. Z. I., Miao, J. J., Lin, S. Y., & Yang, J. H. (2013). *Flow*
9 *visualization, PIV measurement and CFD calculation for fluid-driven natural*
10 *cross-ventilation in a scale model. Energy and Buildings, 66, 306–314.*
11 *<https://doi.org/10.1016/j.enbuild.2013.07.005>*
- 12 [4] Chanteloup, V., & Mirade, P.-S. (2009). *Computational fluid dynamics (CFD)*
13 *modelling of local mean age of air distribution in forced-ventilation food*
14 *plants. Journal of Food Engineering, 90(1), 90–103.*
15 *<https://doi.org/10.1016/j.jfoodeng.2008.06.014>*
- 16 [5] China Association of Building Energy Efficiency(CABEE). (2022). *2022*
17 *Research Report of China Building Energy Consumption and Carbon*
18 *Emissions. China association of building energy efficiency (CABEE).*
19 *<https://www.cabee.org/site/content/24420.html>*
- 20 [6] Duan, J., Li, N., Peng, J., Liu, Q., Peng, T., & Wang, S. (2023). *Clustering and*
21 *prediction of space cooling and heating energy consumption in high-rise*
22 *residential buildings with the influence of occupant behaviour: Evidence from*

- 1 *a survey in Changsha, China. Journal of Building Engineering*, 76, 107418.
2 <https://doi.org/10.1016/j.jobe.2023.107418>
- 3 [7] Franke, J. (2006). *Recommendations of the COST action C14 on the use of*
4 *CFD in predicting pedestrian wind environment. The Fourth International*
5 *Symposium on Computational Wind Engineering, Yokohama, Japan*, 529–532.
- 6 [8] Haghghi, A. P., Pakdel, S. H., & Jafari, A. (2016). *A study of a wind catcher*
7 *assisted adsorption cooling channel for natural cooling of a 2-storey building.*
8 *Energy*, 102, 118–138. <https://doi.org/10.1016/j.energy.2016.02.033>
- 9 [9] Hang, J., & Li, Y. (2011). *Age of air and air exchange efficiency in high-rise*
10 *urban areas and its link to pollutant dilution. Atmospheric Environment*,
11 45(31), 5572–5585. <https://doi.org/10.1016/j.atmosenv.2011.04.051>
- 12 [10] Jiang, F., Tao, S., Tao, Q., Li, zhengrong, Yuan, Y., & Zheng, J. (2022).
13 *The effect of louver blinds on the wind-driven cross ventilation of multi-storey*
14 *buildings. Journal of Building Engineering*, 54, 104614.
15 <https://doi.org/10.1016/j.jobe.2022.104614>
- 16 [11] Kobayashi, T., Sandberg, M., Fujita, T., Lim, E., & Umemiya, N. (2022).
17 *Numerical analysis of wind-induced natural ventilation for an isolated cubic*
18 *room with two openings under small mean wind pressure difference. Building*
19 *and Environment*, 226, 109694.
20 <https://doi.org/10.1016/j.buildenv.2022.109694>
- 21 [12] Kosutova, K., van Hooff, T., Vanderwel, C., Blocken, B., & Hensen, J.
22 (2019). *Cross-ventilation in a generic isolated building equipped with louvers:*

- 1 *Wind-tunnel experiments and CFD simulations. Building and Environment,*
2 *154, 263–280. <https://doi.org/10.1016/j.buildenv.2019.03.019>*
- 3 [13] *Kumar, N., Bardhan, R., Kubota, T., Tominaga, Y., & Shirzadi, M. (2022).*
4 *Parametric study on vertical void configurations for improving ventilation*
5 *performance in the mid-rise apartment building. Building and Environment,*
6 *215, 108969. <https://doi.org/10.1016/j.buildenv.2022.108969>*
- 7 [14] *Kumar, N., Kubota, T., Tominaga, Y., Shirzadi, M., & Bardhan, R. (2021).*
8 *CFD simulations of wind-induced ventilation in apartment buildings with*
9 *vertical voids: Effects of pilotis and wind fin on ventilation performance.*
10 *Building and Environment, 194, 107666.*
11 *<https://doi.org/10.1016/j.buildenv.2021.107666>*
- 12 [15] *Li, Q., Tai, V. C., Moey, L. K., Go, T. F., Safehian, J., & Yazdi, M. H. (2023).*
13 *Impact of planar area ratio and opening positions on natural cross ventilation*
14 *performance in sheltered high-rise buildings: A simulation study. Building and*
15 *Environment, 245, 110889. <https://doi.org/10.1016/j.buildenv.2023.110889>*
- 16 [16] *Liu, J., Heidarinejad, M., Pitchurov, G., Zhang, L., & Srebric, J. (2018).*
17 *An extensive comparison of modified zero-equation, standard k-ε, and LES*
18 *models in predicting urban airflow. Sustainable Cities and Society, 40, 28–43.*
19 *<https://doi.org/10.1016/j.scs.2018.03.010>*
- 20 [17] *Meroney, R. N. (2009). CFD prediction of airflow in buildings for natural*
21 *ventilation.*
- 22 [18] *Moey, L. K., Chan, K. L., Tai, V. C., Go, T. F., & Chong, P. L. (2021).*
23 *Investigation on the effect of opening position across an isolated building for*

- 1 *wind-driven cross ventilation. Journal of Mechanical Engineering and*
2 *Sciences, 15(2), 8141–8152. <https://doi.org/10.15282/jmes.15.2.2021.14.0639>*
- 3 [19] *Moey, L. K., Kong, M. F., Tai, V. C., Go, T. F., & Adam, N. M. (2021).*
4 *Effects of roof configuration on natural ventilation for an isolated building.*
5 *Journal of Mechanical Engineering and Sciences, 15(3), Article 3.*
6 *<https://doi.org/10.15282/jmes.15.3.2021.15.0659>*
- 7 [20] *Moey, L. K., Sing, Y. H., Tai, V. C., Go, T. F., & Ng, J. Y. (2022). Numerical*
8 *investigation of inlet opening size on wind-driven cross ventilation. Journal of*
9 *Mechanical Engineering and Sciences, 16(1), 8662–8672.*
10 *<https://doi.org/10.15282/jmes.16.1.2022.02.0685>*
- 11 [21] *Muhsin, F., Yusoff, W. F. M., Mohamed, M. F., & Sopian, A. R. (2017).*
12 *CFD modeling of natural ventilation in a void connected to the living units of*
13 *multi-storey housing for thermal comfort. Energy and Buildings, 144, 1–16.*
14 *<https://doi.org/10.1016/j.enbuild.2017.03.035>*
- 15 [22] *Najafi Ziarani, N., Cook, M. J., Freidooni, F., & O'Sullivan, P. D. (2023).*
16 *The role of near-façade flow in wind-dominant single-sided natural ventilation*
17 *for an isolated three-storey building: An LES study. Building and Environment,*
18 *235, 110210. <https://doi.org/10.1016/j.buildenv.2023.110210>*
- 19 [23] *National Bureau of Statistics. (2022). China Statistical Yearbook 2022.*
20 *China Statistics Press. <http://www.stats.gov.cn/sj/ndsj/2022/indexch.htm>*
- 21 [24] *Omrani, S., Garcia-Hansen, V., Capra, B. R., & Drogemuller, R. (2017).*
22 *Effect of natural ventilation mode on thermal comfort and ventilation*

- 1 *performance: Full-scale measurement. Energy and Buildings, 156, 1–16.*
2 <https://doi.org/10.1016/j.enbuild.2017.09.061>
- 3 [25] *Ramponi, R., & Blocken, B. (2012). CFD simulation of cross-ventilation*
4 *for a generic isolated building: Impact of computational parameters. Building*
5 *and Environment, 53, 34–48. https://doi.org/10.1016/j.buildenv.2012.01.004*
- 6 [26] *Roache, P. J. (1997). Quantification of uncertainty in computational fluid*
7 *dynamics. Annual Review of Fluid Mechanics, 29(1), 123–160.*
8 <https://doi.org/10.1146/annurev.fluid.29.1.123>
- 9 [27] *Shetabivash, H. (2015). Investigation of opening position and shape on the*
10 *natural cross ventilation. Energy and Buildings, 93, 1–15.*
11 <https://doi.org/10.1016/j.enbuild.2014.12.053>
- 12 [28] *Shirzadi, M., Mirzaei, P. A., & Naghashadegan, M. (2018). Development*
13 *of an adaptive discharge coefficient to improve the accuracy of cross-*
14 *ventilation airflow calculation in building energy simulation tools. Building*
15 *and Environment, 127, 277–290.*
16 <https://doi.org/10.1016/j.buildenv.2017.10.019>
- 17 [29] *Spentzou, E., Cook, M. J., & Emmitt, S. (2019). Modelling natural*
18 *ventilation for summer thermal comfort in Mediterranean dwellings.*
19 *International Journal of Ventilation, 18(1), 28–45.*
- 20 [30] *Tai, V. C., Kai-Seun, J. W., Mathew, P. R., Moey, L. K., Cheng, X., &*
21 *Baglee, D. (2022). Investigation of varying louver angles and positions on*
22 *cross ventilation in a generic isolated building using CFD simulation. Journal*

- 1 of *Wind Engineering and Industrial Aerodynamics*, 229, 105172.
2 <https://doi.org/10.1016/j.jweia.2022.105172>
- 3 [31] Tominaga, Y., & Blocken, B. (2016). *Wind tunnel analysis of flow and*
4 *dispersion in cross-ventilated isolated buildings: Impact of opening positions.*
5 *Journal of Wind Engineering and Industrial Aerodynamics*, 155, 74–88.
6 <https://doi.org/10.1016/j.jweia.2016.05.007>
- 7 [32] Tominaga, Y., Mochida, A., Yoshie, R., Kataoka, H., Nozu, T., Yoshikawa,
8 M., & Shirasawa, T. (2008). *AIJ guidelines for practical applications of CFD*
9 *to pedestrian wind environment around buildings. 4th International*
10 *Symposium on Computational Wind Engineering (CWE2006)*, 96(10), 1749–
11 1761. <https://doi.org/10.1016/j.jweia.2008.02.058>
- 12 [33] US Energy Information Administration. (2021). *Use of energy explained–*
13 *Energy use in homes.*
- 14 [34] van Hooff, T., Blocken, B., & Tominaga, Y. (2017). *On the accuracy of*
15 *CFD simulations of cross-ventilation flows for a generic isolated building:*
16 *Comparison of RANS, LES and experiments. Building and Environment*, 114,
17 148–165. <https://doi.org/10.1016/j.buildenv.2016.12.019>
- 18 [35] van Hooff, T., Blocken, B., & van Heijst, G. J. F. (2013). *On the suitability*
19 *of steady RANS CFD for forced mixing ventilation at transitional slot Reynolds*
20 *numbers. Indoor Air*, 23(3), 236–249. <https://doi.org/10.1111/ina.12010>
- 21 [36] Waheeb, M. I., & Hemeida, F. A. (2022). *Study of natural ventilation and*
22 *daylight in a multi-storey residential building to address the problems of*

- 1 *COVID-19. Technologies and Materials for Renewable Energy, Environment*
2 *and Sustainability*, 8, 863–880. <https://doi.org/10.1016/j.egy.2022.07.078>
- 3 [37] *Yazarlou, T., & Barzkar, E. (2022). Louver and window position effect on*
4 *cross-ventilation in a generic isolated building: A CFD approach. Indoor and*
5 *Built Environment*, 31(6), 1511–1529.
6 <https://doi.org/10.1177/1420326X211061685>
- 7 [38] *Zhang, X., Weerasuriya, A. U., Wang, J., Li, C. Y., Chen, Z., Tse, K. T., &*
8 *Hang, J. (2022). Cross-ventilation of a generic building with various*
9 *configurations of external and internal openings. Building and Environment*,
10 *207, 108447. https://doi.org/10.1016/j.buildenv.2021.108447*
- 11 [39] *Zheng, J., Tao, Q., & Chen, Y. (2022). Airborne infection risk of inter-unit*
12 *dispersion through semi-shaded openings: A case study of a multi-storey*
13 *building with external louvers. Building and Environment*, 225, 109586.
14 <https://doi.org/10.1016/j.buildenv.2022.109586>
- 15 [40] *Zheng, J., Tao, Q., & Li, L. (2020). Numerical study of wind environment*
16 *of a low-rise building with shading louvers: Sensitive analysis and evaluation*
17 *of cross ventilation. Journal of Asian Architecture and Building Engineering*,
18 *19(6), 541–558. https://doi.org/10.1080/13467581.2020.1758113*
- 19 [41] *Zou, C., Zhu, J., Lou, K., & Yang, L. (2022). Coupling coordination and*
20 *spatiotemporal heterogeneity between urbanization and ecological*
21 *environment in Shaanxi Province, China. Ecological Indicators*, 141, 109152.
22 <https://doi.org/10.1016/j.ecolind.2022.109152>
- 23